



Contents lists available at ScienceDirect

Journal of Rock Mechanics and Geotechnical Engineering

journal homepage: www.jrmge.cn

Full Length Article

Linking evolution of heterogeneous microstructure and rheology of granite to 1000 °C

Liyuan Liu ^{a, b, *}, Shengwen Luo ^a, Derek Elsworth ^c, Kai Liu ^d, Yifan Luo ^e, Hongguang Ji ^{a, b}, Tao Wang ^{a, f}

^a Key Laboratory of Ministry of Education for Efficient Mining and Safety of Metal Mines, University of Science and Technology Beijing, Beijing, 100083, China

^b School of Resources and Safety Engineering, University of Science and Technology Beijing, Beijing, 100083, China

^c Departments of Energy and Mineral Engineering & Geosciences, G3 Center, Pennsylvania State University, University Park, PA, 16802, USA

^d Department of Engineering Science, University of Oxford, Parks Road, Oxford, OX1 3PJ, UK

^e Deep Mining Laboratory of Shandong Gold Group Co., Ltd., Yantai, 261400, China

^f School of Future Cities, University of Science and Technology Beijing, Beijing, 100083, China

ARTICLE INFO

Article history:

Received 23 October 2024

Received in revised form

26 March 2025

Accepted 26 March 2025

Available online xxx

Keywords:

High temperature treatment

Thermal damage

Microstructure evolution

Thermal-mechanical-damage coupling

Rock heterogeneity

ABSTRACT

The study of the effects of thermal damage on the mineral components, microstructure, and macroscopic physico-mechanical properties of rocks can provide valuable references for rock engineering design and long-term safety evaluations. In this work, we systematically study the evolution of microstructure and variations in the mechanical properties of granite under high-temperature conditions. The microstructural changes and macro-mechanical properties of rocks are investigated across a temperature range of 25 °C–1000 °C through the application of characterization techniques, macro-mechanical experiments, and numerical simulations. High temperatures induce the gradual evolution of micropores and mesopores into macropores, culminating in a significant increase in porosity, with the most rapid rate of increase occurring at 400 °C. The X-ray diffraction (XRD) results indicate that the high-temperature environment (below 1000 °C) specifically affects the intensity of the maximum diffraction peaks and the half-height width (FWHM) of each mineral component in the granite. The scanning electron microscope (SEM) observation confirms the development of fracture and the reduction in cementation between mineral particles under different temperatures. Additionally, uniaxial and triaxial compression tests were conducted using the GCTS mechanical loading system. Experimental results reveal that the threshold temperature for granite damage is 400 °C, and the temperature range for the brittle-ductile transition of granite lies roughly between 600 °C and 800 °C. Numerical simulations were performed by employing non-homogeneous rock damage theory and a thermal-mechanical-damage coupling model. Simulated results align well with experimental data. Specifically, the simulations demonstrate that high-temperature treatment causes the redistribution of microstructure in granite, resulting in increased heterogeneity and a change in the failure morphology.

© 2025 Institute of Rock and Soil Mechanics, Chinese Academy of Sciences. Published by Elsevier B.V. This is an open access article under the CC BY-NC-ND license (<http://creativecommons.org/licenses/by-nc-nd/4.0/>).

1. Introduction

Subsurface environments at high temperature significantly impact the mechanical properties of rocks (Zhang et al., 2021;

Kumari and Ranjith, 2022). High-temperature cycling poses significant challenges in multiple engineering applications. These include radioactive nuclear waste disposal, deep geothermal resource utilization, in situ gasification and heat transfer in coal and oil shale, ultra-deep reservoir development, and deep oil/gas field exploration. All these engineering systems are vulnerable to damaging thermal strains and structural deterioration during operation. Such processes significantly impact reactions and phase transformations in mineral composition and microstructure as well as the evolution of damage that importantly impact stability (Pathiranagei and Gratchev, 2021; Liu et al., 2021; Alanazi et al.,

* Corresponding author. Key Laboratory of Ministry of Education for Efficient Mining and Safety of Metal Mines, University of Science and Technology Beijing, Beijing, 100083, China.

E-mail address: liuliyuan@ustb.edu.cn (L. Liu).

Peer review under responsibility of Institute of Rock and Soil Mechanics, Chinese Academy of Sciences.

<https://doi.org/10.1016/j.jrmge.2025.03.006>

1674-7755/© 2025 Institute of Rock and Soil Mechanics, Chinese Academy of Sciences. Published by Elsevier B.V. This is an open access article under the CC BY-NC-ND license (<http://creativecommons.org/licenses/by-nc-nd/4.0/>).

2023). Understanding this response is important in prevention of underground fires and the evaluation of the long-term safety of rock engineering in areas characterized by extreme geothermal anomalies.

The physical and mechanical properties of rocks under high-temperature and high-pressure provide key constraints on deep-earth engineering and deep resource exploitation. As one of the most widely distributed rock types on Earth, granite, characterized by its high strength and dense structure, proves to be an excellent engineering material under extreme conditions. Additionally, granite exhibits significant heterogeneous characteristics and is sensitive to temperature changes, which facilitates the study of the mechanisms by which temperature affects its heterogeneous properties. Extensive studies have documented the physical and mechanical transformations of granites under high temperature and high pressure (Kahraman, 2022; Igusheva and Petrov, 2024; Wang et al., 2024). High temperatures induce expansion of mineral particles and alterations in mineral composition, which in turn precipitate the disintegration of the internal structure and concomitant shifts in mechanical parameters (Li et al., 2024). When the heating temperature exceeds 400 °C, the peak stress and elastic modulus of granite decrease significantly with the increasing temperature, while the peak strain increases (Gautam et al., 2018). At 550 °C, thermal cracks initially begin to form, and the mechanical failure under uniaxial compression changes from axial splitting to conjugate shear failure (Jin et al., 2024). After exposure to temperatures exceeding 600 °C, the peak strain of the granite increases and the specimen turns into progressive instability failure, which indicates enhancement in ductility (He et al., 2022). In certain underground projects, environmental temperatures can exceed 800 °C, altering the mineralogical composition of the rock (Ersoy et al., 2019). In regions characterized by extreme geothermal anomalies and uncontrolled underground fires, rocks are exposed to temperatures that can reach 1000 °C (Liu et al., 2025). Consequently, it is necessary to elevate the target temperature for the study. Research on the mechanical properties of granite at temperatures reaching 1000 °C is rather limited, with a focus solely on the variation of physical parameters and the compressive strength, neglecting the comprehensive analysis of other mechanical properties. The effects of temperatures reaching 1000 °C on the nature of granite remain undefined.

The mineral composition, pore size distribution and microfracture density of granites exposed to high temperature generally evolve (Ersoy et al., 2021a, 2021b; Li et al., 2021; Abddaim et al., 2024). Evolution of microcracks using scanning electron microscope (SEM) at different temperatures in the range of 25 °C–800 °C shows extension of intrinsic microcracks that eventually coalesce to form macrocrack networks. This intrinsically weakens the structure through rock damage and rupture (Liu et al., 2022). Observation of the pore structure of granite at different temperatures through NMR experiments reveals that increasing the temperature leads to an increase in porosity and pore enlargement, ultimately resulting in a decrease in rock strength (Chen et al., 2021; Wu et al., 2023). By combining several characterization techniques, it is possible to uncover the principles behind granite variability at both macroscopic and microscopic levels (Kumari et al., 2019). For example, integrating the results of X-ray diffraction (XRD) and SEM experiments shows that the thermal expansion of various minerals during thermal cycling is a critical factor in causing structural damage (Gautam et al., 2021). Although extensive research has examined variations in physical parameters and mechanical properties of high-temperature granite, systematic investigations remain scarce. Specifically, integrated analyses of both macroscopic characteristics (e.g. basic physical parameters, thermodynamic constants, mechanical parameters) and microscopic features (mineral

compositions, pore-fracture structures, microstructural evolution) are notably lacking.

Conventional tests suffer the inherent limitation of non-repeatability and lack of direct observation of the interaction between multiple processes that contribute to damage. For example, these include the impact of thermal stresses on thermal microcracks. Conversely, numerical studies are eminently repeatable but may not include the full range of physical interactions (Liu et al., 2020; Hart and Rimoli, 2023; Nie et al., 2023). Many numerical models have successfully simulated the deformation and rupture processes of granite after high-temperature treatment (Li and Zhang, 2024; Sun et al., 2021). However, the impact of inhomogeneity on the thermomechanical behavior of granite requires further quantification. The homogeneity of granite is crucial to numerical results due to its varying mineral compositions and pre-existing discontinuities (Meng et al., 2018). Current numerical models represent homogeneity in various ways, such as through mineral compositions and pre-existing discontinuity surfaces (Li et al., 2022) or random finite clusters of elements (Saksala, 2021). Most numerical models use stochastic distribution to represent homogeneity but do not adequately consider its evolution during the heating process.

This study aims to address the knowledge gap regarding linking evolution of heterogeneous microstructure and rheology of granite to 1000 °C. We examine the evolution of damage in granite at high temperatures by exposing samples to progressively increased temperatures. We utilize nuclear magnetic resonance (NMR) to determine the pore size distribution characteristics of granite at various temperatures, aiming to understand the effect of temperature on the pore structure. Additionally, we analyze the evolution of mineral components and microstructure using XRD and SEM before conducting destructive testing in uniaxial and triaxial modes to obtain the rheological properties at different temperatures and confining pressures. We use these observations to determine threshold temperatures for the brittle-ductile transformation. A dual damage TM(D) coupling model is then developed and implemented in COMSOL Multiphysics with MATLAB to represent this response. Inversion of a homogeneity index by the TM(D) coupling model was used to study the variation of granite heterogeneity with temperature. Experiments and numerical simulations comprehensively explore microstructural changes and macro-mechanical behavior of granite in high-temperature environments. These studies enhance understanding of high-temperature rock behavior, particularly the changes in the microscopic and macroscopic mechanical properties of granite at 1000 °C. This research also provides valuable data for future deep-earth engineering in regions with extremely high temperatures.

2. Experimental protocol

Granite samples are exposed to varying temperatures and exposure times at different elevated temperatures. A portion of the rock samples is vacuum saturated with water, and NMR experiments are conducted on these saturated samples to observe the effect of temperature on the pore structure. These samples are then subjected to uniaxial and triaxial compression at room temperature to determine the evolution of damage and resulting rheology. After the mechanical tests, XRD and SEM experiments are conducted on the samples to analyze the microstructural changes.

2.1. Sample preparation

A total of 60 cylindrical cores (25 mm in diameter and 50 mm in height) of granite are cored from a single block to maintain consistency. All samples are of greyish-white granite with a density of

approximately 2.576 g/cm^3 , thermal conductivity of 2.997 W/(m K) , thermal diffusion coefficient of $1.752 \text{ mm}^2/\text{s}$, and longitudinal wave velocity of 4653 m/s . The samples are visibly free of defects and large cracks.

The evolution of mechanical properties is tracked under thermal pre-treatment at high temperatures. Starting at room temperature, we gradually increase the temperature up to $1000 \text{ }^\circ\text{C}$. The specific temperatures are $25 \text{ }^\circ\text{C}$, $200 \text{ }^\circ\text{C}$, $400 \text{ }^\circ\text{C}$, $600 \text{ }^\circ\text{C}$, $800 \text{ }^\circ\text{C}$, and $1000 \text{ }^\circ\text{C}$. Triaxial compression experiments are conducted at confining stresses of 0 MPa , 10 MPa , and 20 MPa .

2.2. Heat treatment methods

A KSL-1700X muffle furnace is used for heat treatment of the specimens, where 5 of 6 sample groups are heated to $200 \text{ }^\circ\text{C}$, $400 \text{ }^\circ\text{C}$, $600 \text{ }^\circ\text{C}$, $800 \text{ }^\circ\text{C}$ and $1000 \text{ }^\circ\text{C}$, respectively. Samples are heated at $5 \text{ }^\circ\text{C}/\text{min}$ to the target temperature, and then held constant for 200 min before being cooled at the same rate (Fig. 1). After uniform cooling to room temperature, mass, size and longitudinal wave velocities are measured. Apparent morphology of the rock samples changes after heat treatment with a change in color from light grey to white, the presence of a powdered surface, signs of crystal detachment and an audible dampening/sharpening in collision (Fig. 2b). At $200 \text{ }^\circ\text{C}$ and $400 \text{ }^\circ\text{C}$, the loss of moisture lightens the surface color, and the area coverage of biotite on the surface is significantly reduced. At temperatures above $600 \text{ }^\circ\text{C}$, the sample becomes almost completely dry, with some minerals oxidizing and expansion cracks (Fig. 2d and e) appearing on the rock surface, which further expand with increasing temperatures. At $800 \text{ }^\circ\text{C}$ and $1000 \text{ }^\circ\text{C}$, some samples may even fragment (Fig. 2e and f).

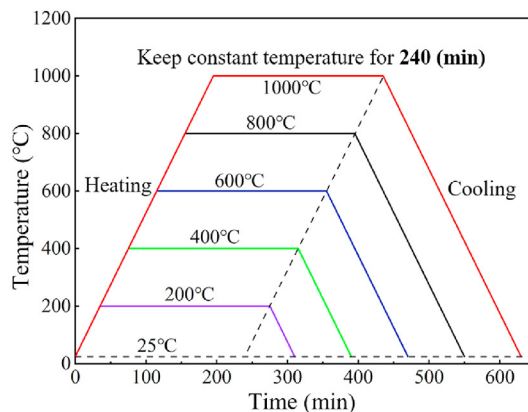
2.3. Experimental procedure

The workflow for the experimental suite is shown in Fig. 3, with specific experimental procedures as follows:

- (1) Measure the grouped and numbered granite samples using a balance and caliper to obtain their mass, height, and diameter. Select six samples from each temperature group and measure their longitudinal wave speeds at room temperature. Afterward, perform the heat treatment for the samples.



(a)



(b)

Fig. 1. Muffle furnace and temperature path followed in thermal treatment: (a) KSL-1700X muffle furnace, and (b) Programmed heating and cooling path for the granite.

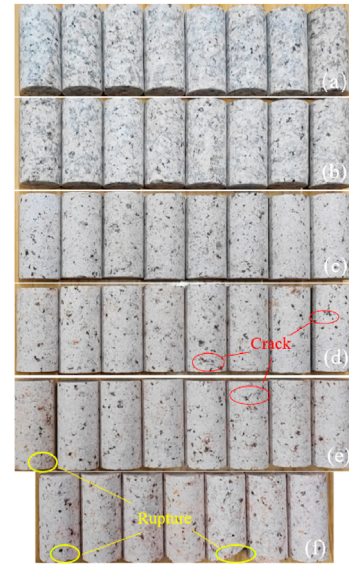


Fig. 2. Exterior morphology of samples after high-temperature heat treatments: (a) $25 \text{ }^\circ\text{C}$, (b) $200 \text{ }^\circ\text{C}$, (c) $400 \text{ }^\circ\text{C}$, (d) $600 \text{ }^\circ\text{C}$, (e) $800 \text{ }^\circ\text{C}$, and (f) $1000 \text{ }^\circ\text{C}$.

Re-measure their masses, heights, diameters, and wave speeds post-treatment.

- (2) Uniaxial and triaxial compression tests are performed using GCTS testing systems to determine the stress-strain behavior until failure. Each temperature and confining pressure condition is tested three times, producing complete and consistent results that align with the data set used for subsequent analysis.
- (3) A single sample from each confining stress and heat-treatment temperature is selected for hot-disk thermodynamic constant measurements, totaling 18 samples. This process recovers thermal conductivities and diffusivities.
- (4) The previously selected rock samples for NMR experiments are vacuumed and saturated with water. NMR experiments are conducted once the samples reach a saturated state. The samples are then placed in a dry and ventilated area for one month to prevent water from affecting future experiments.

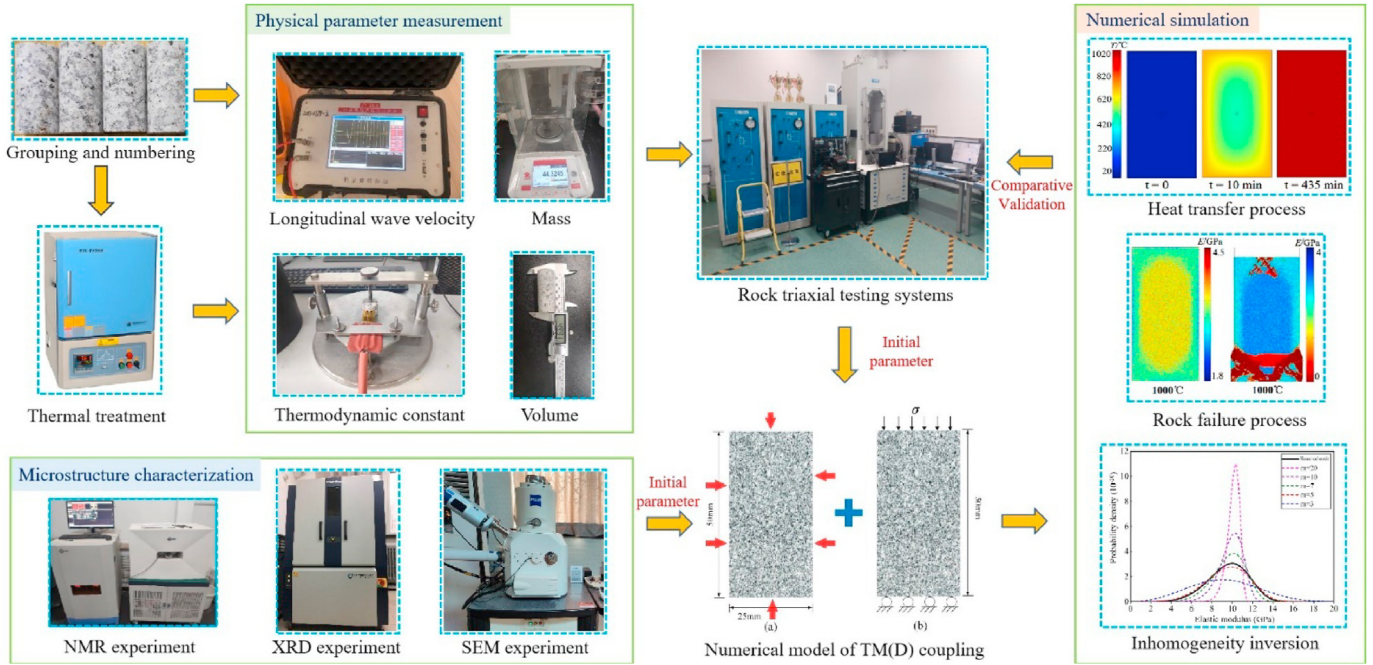


Fig. 3. Workflow for the suite of experiments.

- (5) A single sample from each pre-treatment temperature is powdered and used for XRD analysis, totaling six samples, to determine mineralogical composition.
- (6) A single sample from uniaxial testing for each pre-treatment temperature is sectioned for SEM to examine microstructural changes resulting from heat treatment.

3. Results and analysis

The fundamental physical properties of granite are measured to study how these properties vary with temperature. XRD, NMR, and SEM are used to examine the evolution of mineral components, porosity, pore size distribution, and microfracture pore structure with temperature. The results of uniaxial and triaxial tests are analyzed to understand the evolution of mechanical parameters under different temperatures and confining pressures.

3.1. Physical changes with heat treatment

Changes in the mass, volume and density of the granite with temperature are summarized in Fig. 4. The mass of granite decreases gradually with the increase in temperature, but the change is relatively small. As the temperature increases, the measurement data become more dispersed. This can be attributed to the fact that at high temperatures, the effects on the various physical properties of granite vary more significantly. The changing rate of granite volume increases with the increase in temperature. Between 400 °C and 600 °C, as the oxidative decomposition of mineral particles within the rock produces new microporous microcracks, the quartz undergoes a phase transition to increase the volume, as well as the primary pore cleavage within the rock continues to expand and develop, resulting in a rapid increase in the volume of the rock. When the temperature exceeds 800 °C, the internal pore space of the rock further expands and the cracks continue to extend, leading to larger cracks on the surface and even fracture. The density of granite decreases with the increase in temperature, but the change is small compared with the volume, and it is only reduced by 0.42%

at 1000 °C. Therefore, the change of granite density is mainly affected by the expansion of volume. Based on the above observation, 400 °C can be taken as the threshold temperature for the changes of granite mass, volume and density.

The longitudinal wave velocity of granite treated by different high temperatures is shown in Fig. 5. When exposed to the higher temperature, longitudinal wave velocity decreases gradually. With the increase of temperature, the loss of free water in the internal pores of the rock and structural water in the mineral grains leads to a decrease in the tightness of the cementation between the rock particles, while microcracks begin to increase and widen, thus affecting the propagation of longitudinal wave signals through the rock.

The thermal conductivity of heat-treated granite is determined by using a hot-disk thermal constant analyzer model TPS2500. Thermodynamic constants of granite at different temperature conditions are obtained and fitted experimentally, as shown in Fig. 6. It is observed that the thermal conductivity and thermal diffusion coefficient of granite show a uniform decrease with the increase in temperature. The average thermal conductivity decreased from 2.997 W/(m K) to 1.136 W/(m K), a decrease of 62.1%; the thermal diffusion coefficient decreased from 1.752 mm²/s to 0.718 mm²/s, a decrease of 59%. Besides, it can be seen that the thermodynamic constants of granite are linearly decreasing with the increase of temperature, and the equations of λ and α versus temperature T can be obtained by fitting:

$$\lambda = -0.00196T + 3.125 \quad (R^2 = 0.989) \quad (1)$$

$$\alpha = -0.00104T + 1.774 \quad (R^2 = 0.982) \quad (2)$$

The evolution trends of granite mass, volume, density, wave velocity, thermal conductivity, thermal diffusion coefficient and other parameters with temperature show that there are obvious differences in the sensitivity of different parameters to temperature. The absolute rates of change of each parameter at 1000 °C are

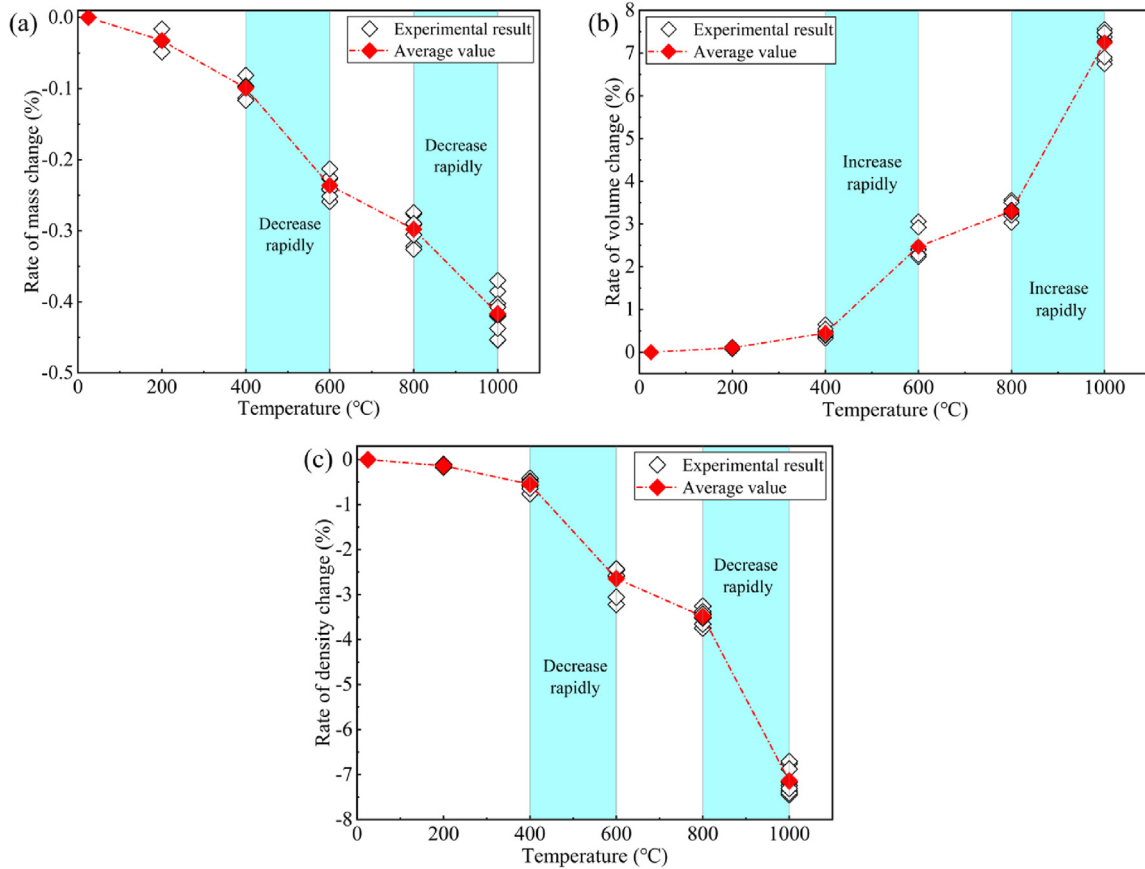


Fig. 4. Rates of change in physical parameters for heat-treated granite samples from pre- to post-treatment.

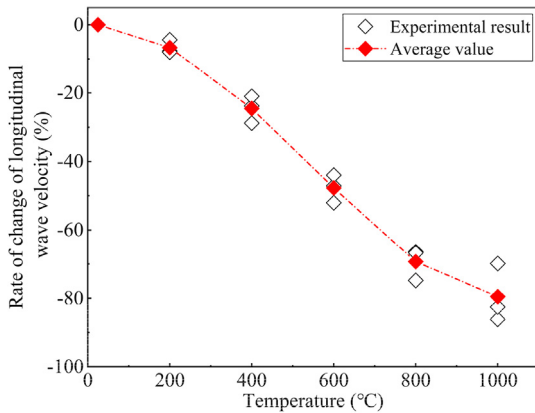


Fig. 5. Variation in rate of change of longitudinal wave speed with temperature.

compared, as listed in Table 1. The sensitivity of each physical parameter to temperature is in the following order from strongest to weakest: longitudinal wave velocity > thermal conductivity > thermal diffusion coefficient > volume > density > mass.

3.2. Mineralogical and microstructural changes with heat-treatment

3.2.1. Pore size distribution characteristics

Fig. 7a shows the T_2 spectrum distribution curves of granite after exposure to high temperature. The T_2 spectrum distribution reflects the variations in pore structure following high-temperature

treatment. All T_2 spectrum curves display smooth and continuous characteristics, indicating robust connectivity among pores within granite. From the perspective of the horizontal axis, the T_2 spectrum of granite exhibits a systematic rightward shift with increasing temperature, suggesting a gradual increase in the pore diameter of its internal pores. Conversely, from the vertical axis perspective, the overall upward trend observed in the T_2 spectrum indicates that as temperature rises, there is an observable increase in the number of internal pores within granite.

Through the analysis of porosity and pore volume ratio at each temperature, the cumulative pore volume ratio for different sizes is determined, as illustrated in Fig. 7b. It can be observed that the porosity of granite increases more rapidly with rising temperature. The figure shows that the volume ratio of micropores and mesopores initially decreases and then increases with temperature. Conversely, the volume ratio of macropores steadily increases as the temperature rises.

When the temperature is below 400 °C, the volume ratio of micropores and mesopores decreases, primarily due to the slow development of these pores through thermal damage and the formation of new mesopores and macropores. Beyond 400 °C, the volume ratio of micropores and mesopores gradually increases, indicating the formation of new micropores within the granite, along with a significant number of mesopores and macropores. Consequently, between 400 °C and 800 °C, the growth rate of granite porosity progressively increases. At 1000 °C, there is a further increase in porosity as micropores, mesopores, and macropores continue to expand. This observation suggests that 400 °C is the threshold temperature at which the porosity of granite undergoes significant changes.

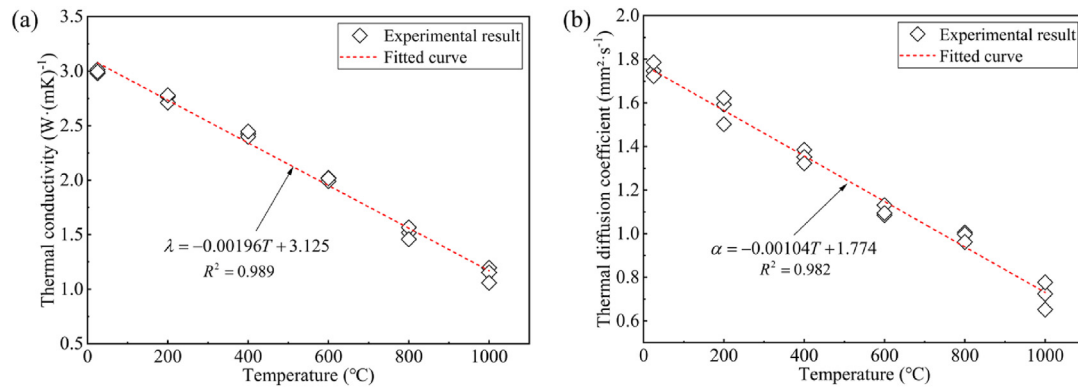


Fig. 6. Variation in thermodynamic parameters with temperature for granite post-treatment.

Table 1
Absolute values of the rate of change of each parameter at 1000 °C.

Mass (%)	Volume (%)	Density (%)	Longitudinal wave velocity (%)	Thermal conductivity (%)	Thermal diffusion coefficient (%)
0.42	7.24	7.14	79.49	62.1	59

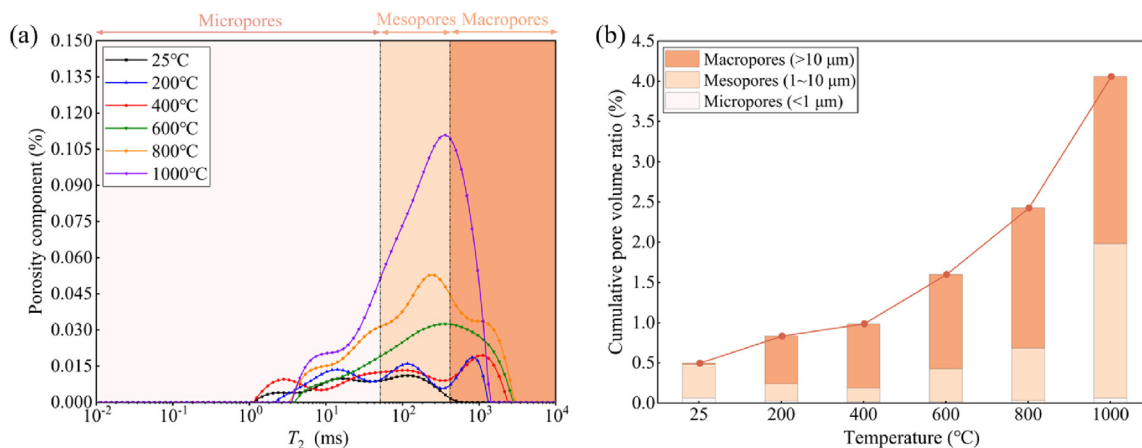


Fig. 7. Pore size distribution characteristics of granite after high-temperature treatment.

3.2.2. Mineralogical changes

Fig. 8 shows the XRD diffraction patterns of granite under different temperature conditions. It is observed that the main mineral components of granite do not change under high-temperature environment, but the intensity of the diffraction peaks has obvious changes, especially at ultra-high temperature.

The peaks marked with green bold font in Fig. 8 are the maximum diffraction peaks corresponding to each mineral. The diffraction angles of each mineral do not change significantly at different temperatures. When the temperature ascends to 200 °C, the diffraction intensity of quartz experiences a significant increase and remains at a relatively high level within the temperature range of 200 °C–1000 °C. This phenomenon is closely associated with the alterations in the symmetry of the crystal structure and the atomic arrangement pattern during phase transformation. The half-height width of the maximum diffraction peak of quartz is stable at about 0.143.

The intensity of the maximum diffraction peak of calcium feldspar has a tendency to increase slowly up to 800 °C, but it suddenly decreases from 3362 to 2417 at 1000 °C, and the half-height width increases rapidly to 0.236, which indicates that the

crystal structure of calcium feldspar is affected by the temperature exceeding 800 °C. The intensity of the diffraction peaks of potassium feldspar increases gradually with the increase of temperature, while the half-height width shows a trend of decreasing. In particular, the diffraction intensity of potassium feldspar increases from 6710 at 600 °C to 11,060 at 800 °C, which is associated with the transformation of potassium feldspar into its poorly-property homomorphic polymorph anorthoclase. With the increase of temperature, the diffraction peak intensity of sodium feldspar has a tendency to increase and then decrease, and the half-height width has a tendency to decrease and then increase. At 400 °C, the crystal structure is the best.

High temperature induces alterations in rock mineral composition and structure, and these alterations result in thermal damage, with the transformation of feldspar being a crucial factor (Peng et al., 2024). As temperature increases, feldspar minerals within granite decompose into clay minerals, thereby leading to the degradation of the macroscopic mechanical properties of specimens. Notably, the significant increase in thermal damage after 400 °C is attributed to the decomposition of albite under high-temperature conditions. The crucial factor contributing to the

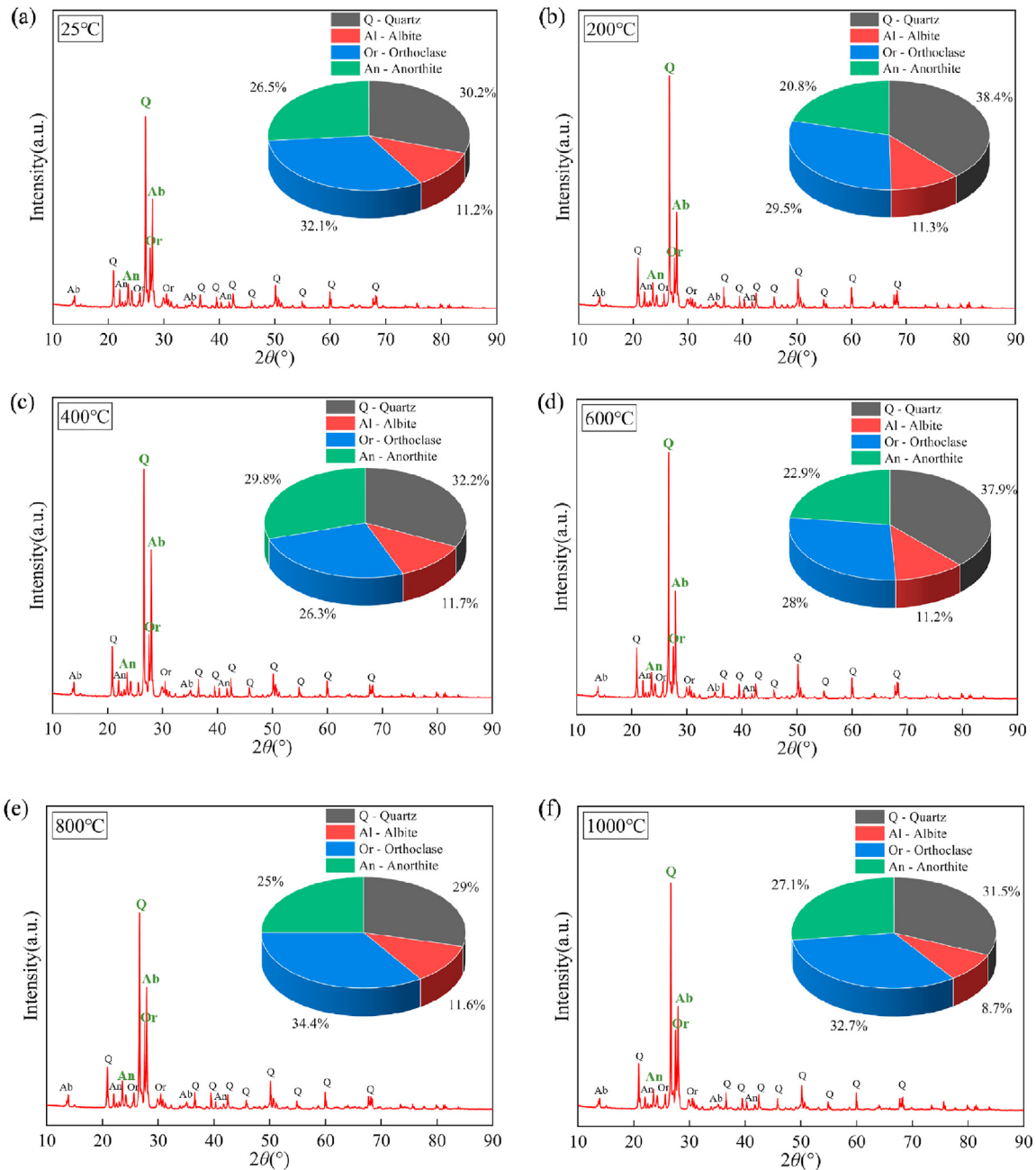


Fig. 8. XRD diffraction patterns for granite under different pre-treatment temperatures: (a) 25 °C, (b) 200 °C, (c) 400 °C, (d) 600 °C, (e) 800 °C, and (f) 1000 °C.

brittle-ductile transformation of granite within the temperature range of 600 °C–800 °C is the conversion of potassium feldspar into plagioclase under the influence of temperature.

3.2.3. Microstructural evolution

Fig. 9 shows the SEM images of granite at room temperature (25 °C), 200 °C, 400 °C, 600 °C, 800 °C and 1000 °C, respectively. At room temperature, the mineral particles on the surface of the granite samples are in close contact with each other and exhibit consistent shapes with no obvious differences. When the temperature increases to 200 °C, large mineral particles are observed, and small inter-granular cracks appear between them. At this stage, the influence of temperature on granite is found to be negligible, with no substantial changes observed in the microstructure of sample surface. At 400 °C, the cracks on the rock surface become further

visible, and the pore fissures between the large minerals are enlarged. The pronounced emergence of surface cracks also serves as indirect evidence that 400 °C represents the threshold temperature for rock damage. At 600 °C, the minerals on the rock surface form a uniform scaly texture, and the number of microcracks and pores is significantly increased. When the temperature reaches 1000 °C, it can be observed that there are obvious cracks on the surface of the rock, and the large minerals are broken into minerals of different sizes by the high temperature, and the mineral particles are loose. The numbers of cracks and pores increase significantly due to the obvious decrease in the degree of cementation between each other. Combined with the XRD observation, the integrity of the calcium feldspar crystal structure may be deteriorated by heat, and the particle size becomes smaller. It is found that the effect of high temperature causes a series of physicochemical changes in

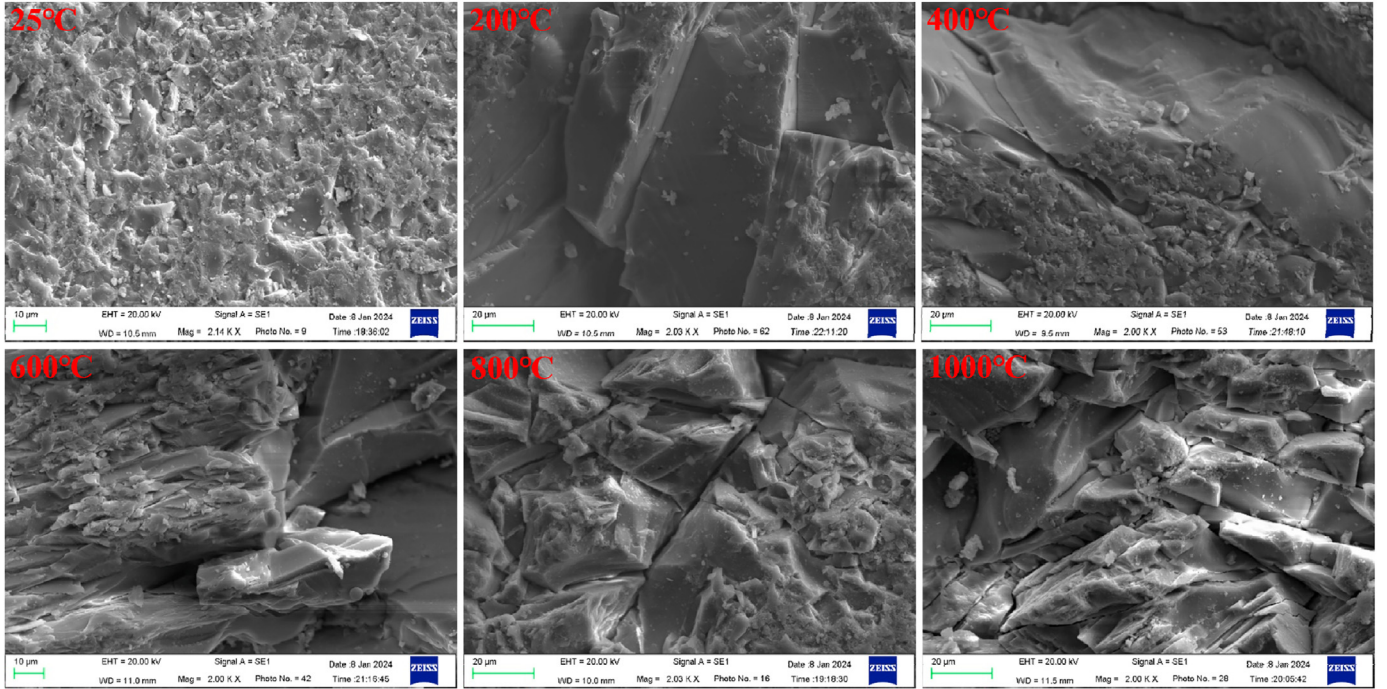


Fig. 9. SEM images of the granite subjected to different pre-treatment temperatures.

mineral particles, such as phase transformation, volume expansion and decomposition, which lead to the generation of cracks in granite. Additionally, this phenomenon will be further intensified as the temperature rises.

3.3. Evolution of mechanical properties

Fig. 10 shows the uniaxial and triaxial stress-strain curves of granite subjected to different high temperatures. It is obvious that the higher the temperature, the greater the effect on the stress-strain curve of granite. With increasing temperature, both uniaxial and triaxial strength of rock roughly show a decreasing trend, while the axial and radial peak strains exhibit an increasing trend. The confining pressure also has a certain effect on the stress-strain curve of granite, observed by the phenomenon that strength increases significantly with the increase in confining pressure under different temperature conditions.

The stress and strain of rock in the elastic deformation phase are proportional to each other, and the proportionality coefficient is called elastic modulus. There are some special cases where it is difficult to determine the linear elastic phase from the stress-strain curve to calculate the rock elastic modulus, thus the deformation modulus E_{50} is used instead of the elastic modulus E with the following formula:

$$E_{50} = \frac{\sigma_{50}}{\varepsilon_{50}} \quad (3)$$

where σ_{50} is 50% of the peak stress in the rock, and ε_{50} is the corresponding strain on the stress-strain curve.

The changes of peak stress, damage stress, elastic modulus, deformation modulus and Poisson's ratio of granite under different temperatures and confining pressures are shown in Fig. 11. The higher the temperature, the smaller the elastic modulus and deformation modulus of granite, and the elastic modulus is always greater than the deformation modulus. The damage factor rises with the increase in temperature, and the change rates of elastic

modulus, deformation modulus and damage factor are obviously accelerated when the temperature is greater than 400 °C. Poisson's ratio decreases smoothly and uniformly with increasing temperature. As shown in Fig. 12a, the cohesion and internal friction angle of granite show a tendency to decrease with increasing temperature, and their rates of change are significantly accelerated above 800 °C. In terms of confinement effect, most of the parameters show an increasing trend with the increase of confining pressure except for Poisson's ratio, the cohesion, and angle of internal friction.

In order to clearly describe the effect of high and low temperatures on the mechanical properties of rocks, some scholars have described the changes in the internal damage characteristics of rocks through the elastic modulus before and after high temperatures (Yang et al., 2019; Liu et al., 2020; Xi et al., 2022). The thermal damage factor is defined as

$$D_T = 1 - \frac{E_T}{E_0} \quad (4)$$

where E_T and E_0 are the elastic moduli of granite at temperature T and 25 °C, respectively (GPa).

As shown in Fig. 12b, the growth rate of the damage factor at 400 °C is significantly higher under uniaxial compression, which also confirms that 400 °C is the threshold temperature for peak stress and damage stress in granite.

The ductility of rock is the property that rock can deform without fracturing when subjected to a sustained stress. This property occurs roughly at the stage of unstable rupture development which begins at the yield point, when the rock sample cracks begin to develop rapidly and gradually penetrate, and the rock strain rate is significantly accelerated but the stress is still slowly rising, finally reaching the peak stress. The ductility of rock is a crucial property to judge the plastic and brittle damage of rock. Therefore, in order to study the damage characteristics of rock, many scholars have defined the ductility coefficient as follows (Xie et al., 2021):

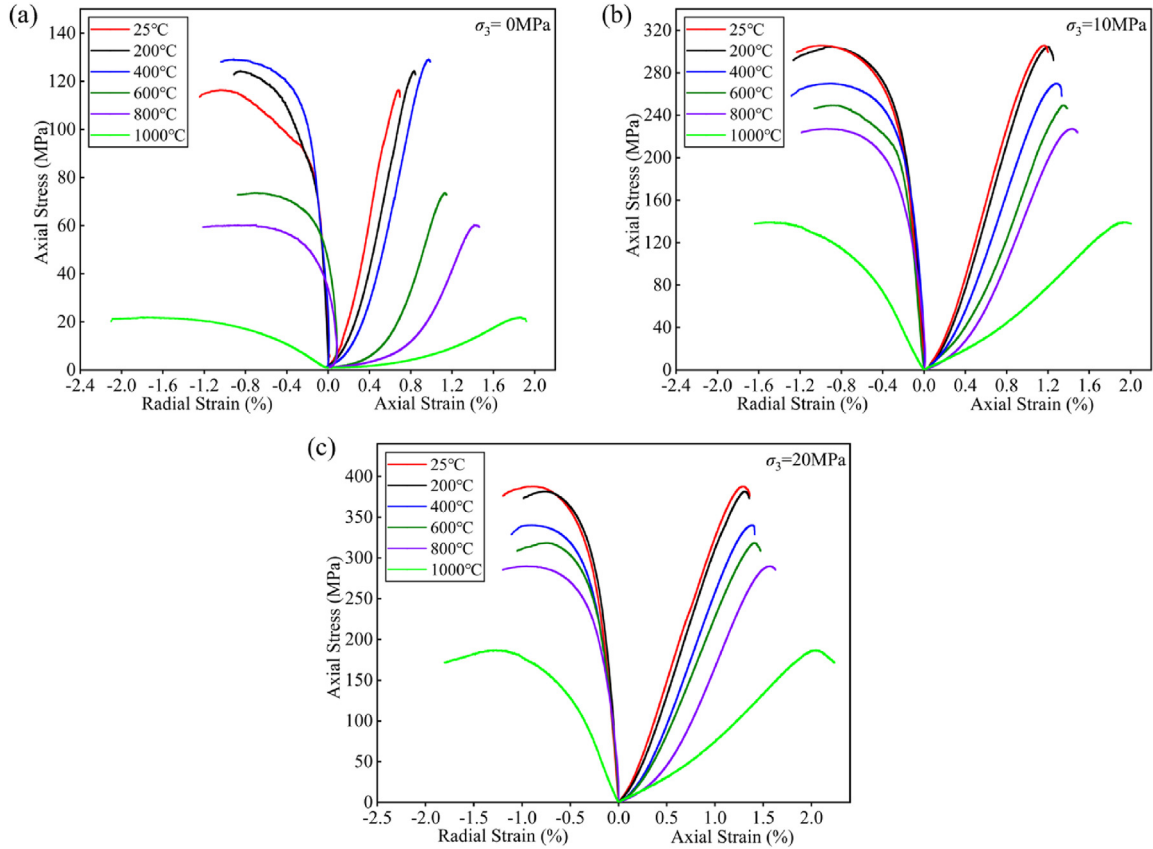


Fig. 10. Uniaxial and triaxial stress-strain curves for different pre-treatment temperatures and at confining pressures of (a) $\sigma_3 = 0$ MPa, (b) $\sigma_3 = 10$ MPa, and (c) $\sigma_3 = 20$ MPa.

$$Y = \frac{\epsilon_c}{\epsilon_{cd}} \quad (5)$$

where ϵ_c is the peak axial strain of granite, and ϵ_{cd} is the yield strain of granite.

The ratios of damage stress to peak stress and ductility coefficients of granite under different confining pressures are shown in Fig. 13a. The ratio of damage stress to peak stress remains stable with the increase of temperature, and then decreases rapidly after 600 °C, which indicates that the ductility of the rock increases in the temperature range of 600 °C–1000 °C. The ductility coefficient of granite increases rapidly when the temperature exceeds 800 °C. The temperature range of brittle-ductile transition of granite is considered to be 600 °C–800 °C.

In this paper, the rock samples are subjected to the above experiments after heat treatment. However, in practical engineering scenarios, rocks are under in situ high temperature and confinement conditions and respond to engineering disturbances. Therefore, future research work should focus on the evolution of microstructure and variations in the mechanical properties of granite under in situ extremely high temperature conditions. Such studies will further deepen the understanding of rock mechanical behaviors and provide a more solid and reliable theoretical basis and data support for practical engineering applications.

4. Coupled modeling of thermo-mechanical (damage)

Based on the meso-statistical mechanics theory of the Weibull distribution, a dual-damage coupled TM(D) model is constructed. The evolution law of thermal damage and the mechanism of changes in rock mechanical properties are analyzed. Finally, the

variation of rock heterogeneity with temperature is quantitatively analyzed through numerical inversion.

4.1. Governing equations

The general equation for heat transfer in rocks is

$$\lambda \nabla^2 T + Q = \rho C \frac{\partial T}{\partial t} \quad (6)$$

where λ is the thermal conductivity, Q is the source term, ρ is the equivalent density, C is the specific heat capacity, and t is the heating time.

The controlling equation for the deformation of rocks affected by temperature is

$$G u_{i,kk} + \frac{G}{1-2\nu} u_{k,ki} - \frac{2G(1+\nu)}{1-2\nu} \alpha_T T_{,i} + f_{,i} = 0 \quad (7)$$

where G is the equivalent shear modulus of the rock, ν is the Poisson's ratio, $u_{i,kk}$ is the second-order derivative of the displacement in the i -direction of the rock u_i in the k -direction, α_T is the coefficient of thermal expansion ($^{\circ}\text{C}^{-1}$), and f_i is the component of body force.

As shown in Fig. 14, when the stress state of the rock satisfies the maximum tensile stress criterion or the Mohr-Coulomb criterion, it undergoes tensile damage or shear damage, respectively, which can be expressed as (Zhu and Tang, 2004):

$$F_1 = -\sigma_3 - f_{t0} = 0 \quad (8)$$

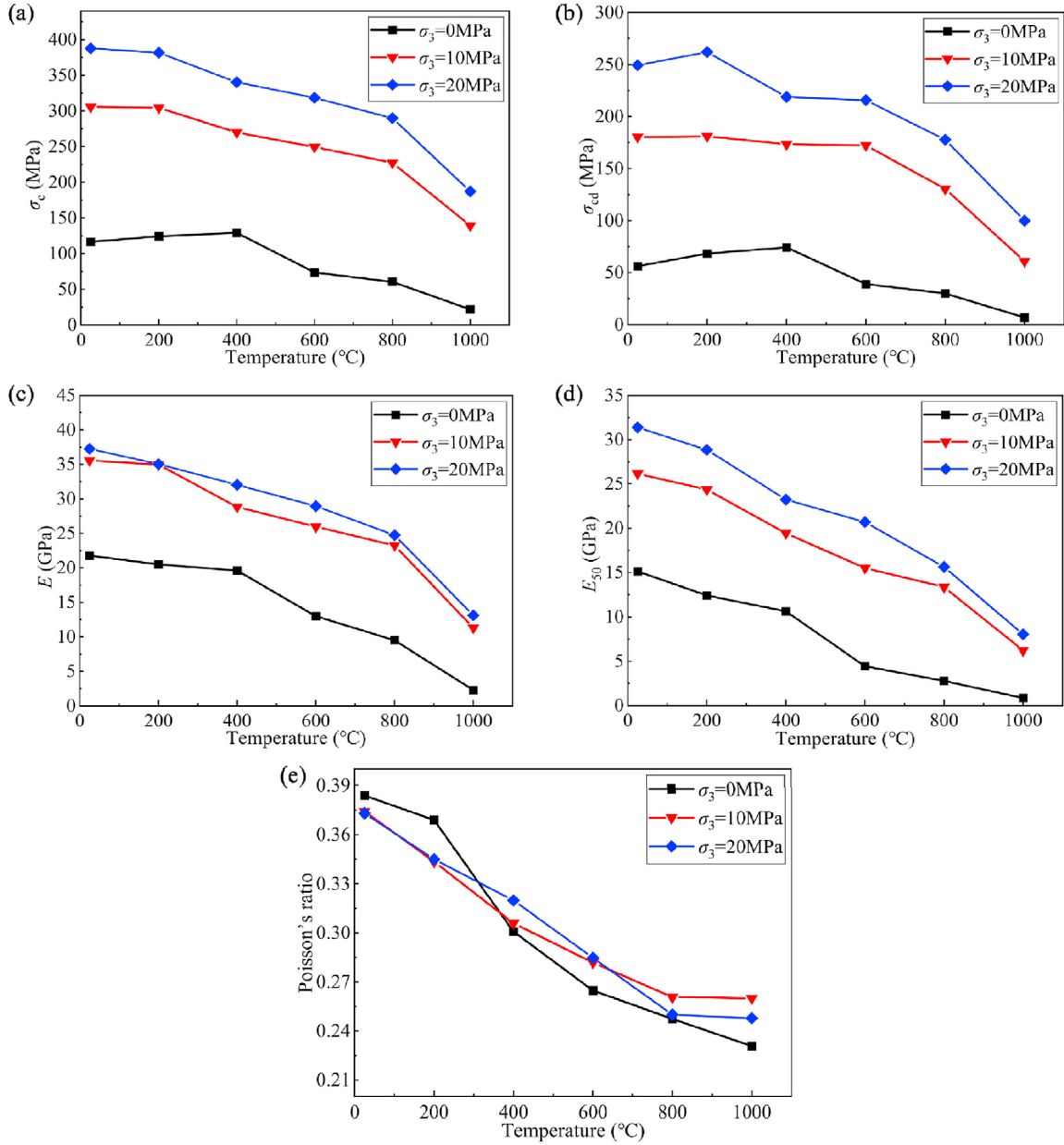


Fig. 11. Variations in strength and deformability for different pre-treatment temperatures and at variable confining pressures.

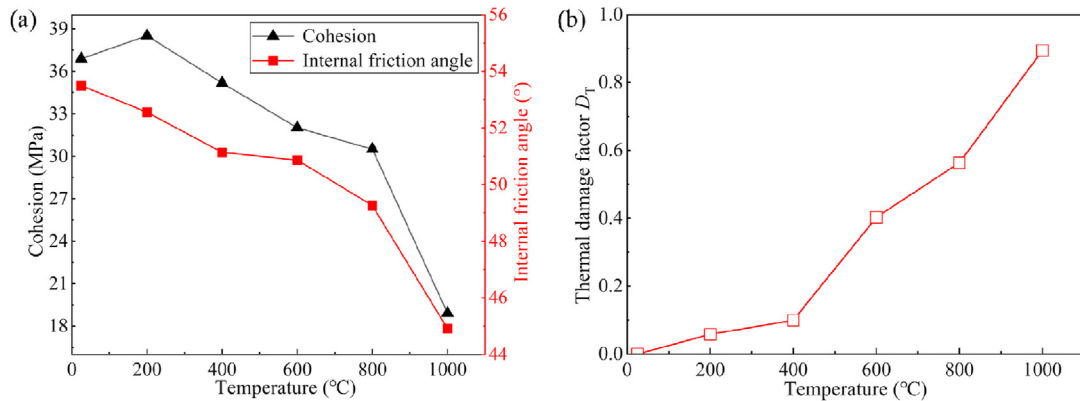


Fig. 12. Variations in mechanical parameters for different pre-treatment temperatures: (a) Cohesion and internal friction angle, and (b) Thermal damage factor.

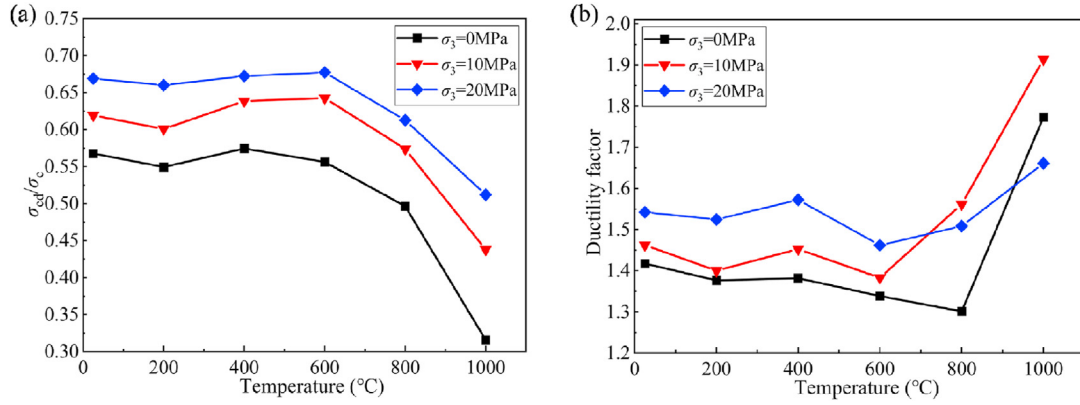


Fig. 13. Changes in ductility with pre-treatment temperature: (a) Ratio of damage stress to peak stress, and (b) Ductility factor.

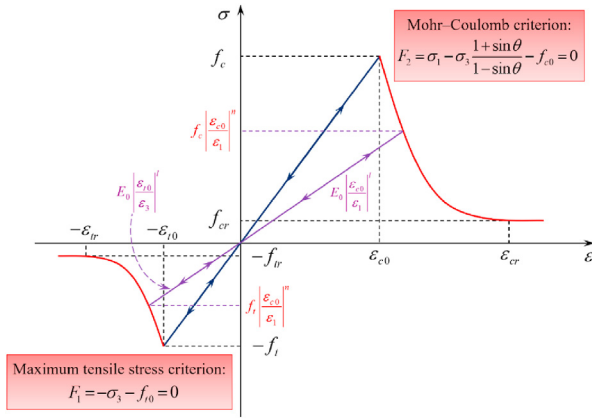


Fig. 14. Damage-based constitutive law in stress-strain space.

$$F_2 = \sigma_1 - \sigma_3 \frac{1 + \sin \varphi}{1 - \sin \varphi} - f_{c0} = 0 \quad (9)$$

where f_{t0} and f_{c0} are the uniaxial tensile and uniaxial compressive strengths of the unit, respectively; σ_1 and σ_3 are the first and third principal stresses, respectively; φ is the internal friction angle; and F_1 and F_2 are the damage threshold functions, respectively.

In Eqs. (8) and (9), the rock stress neither satisfies the maximum tensile stress criterion nor the Mohr-coulomb failure criterion at $F_1 < 0$ and $F_2 < 0$. The stress state satisfies the maximum tensile stress criterion and the tensile damage mode at is still in the loading state. $F_1 = 0$ and $dF_1 > 0$, the stress state satisfies the maximum tensile stress criterion and is a tensile damage mode, and the rock is still in the loading state. $F_2 = 0$ and $dF_2 > 0$, the stress state satisfies the Mohr-Coulomb failure criterion, it is a shear damage mode, and the rock remains in the loaded state.

The damage variable for the rock strength can be calculated as

$$D_s = \begin{cases} 0 & (F_1 < 0 \text{ and } F_2 < 0) \\ 1 - \left| \frac{\epsilon_{t0}}{\epsilon_3} \right|^n & (F_1 = 0 \text{ and } dF_1 > 0) \\ 1 - \left| \frac{\epsilon_{c0}}{\epsilon_1} \right|^n & (F_2 = 0 \text{ and } dF_2 > 0) \end{cases} \quad (10)$$

where ϵ_1 is the maximum principal strain, ϵ_3 is the minimum principal strain, ϵ_{t0} is the maximum tensile strain at the onset of tensile damage, ϵ_{c0} is the maximum compressive strain at the onset

of shear damage, d_s is the damage variable for the rock strength, and n is a constitutive coefficient for rock strength.

According to the elastic damage theory, the elastic modulus of the damaged rock is expressed as

$$E_d = E_0(1 - D_e) = \begin{cases} E_0 & (F_1 < 0 \text{ and } F_2 < 0) \\ E_0 \left| \frac{\epsilon_{t0}}{\epsilon_3} \right|^l & (F_1 = 0 \text{ and } dF_1 > 0) \\ E_0 \left| \frac{\epsilon_{c0}}{\epsilon_1} \right|^l & (F_2 = 0 \text{ and } dF_2 > 0) \end{cases} \quad (11)$$

where D_e is the damage variable applied to the elastic modulus, l is the elastic modulus damage evolution coefficient of granite, E_0 is the elastic modulus of undamaged granite, and E_d is the elastic modulus of granite after damage.

4.2. Fine-scale heterogenous modeling

4.2.1. Coupled TM modelling

The damage of granite induced by heating and uniaxial compression can be simulated by dual damage TM(D) coupling model which is established by COMSOL Multiphysics with MATLAB numerical simulation platform, and is roughly divided into two stages. The first stage is the high-temperature heat treatment stage of granite, as shown in Fig. 15a. By using the heating-holding-cooling path in Fig. 1, it is capability to simulate the heating and holding cooling process. The second stage simulates the uniaxial compression test, as in Fig. 15b. Subsequently, based on the finite element software COMSOL Multiphysics, the fully coupled rock thermal-mechanical-damage (TMD) process can be realized using MATLAB programming.

4.2.2. Representation of heterogeneity

The non-homogeneity of rocks has a significant effect on the damage evolution of rocks (Lan et al., 2013). In order to characterize the inhomogeneity at the fine-scale level, mechanical parameters such as elastic modulus and strength can be assigned according to the Weibull distribution. This distribution defines parameters according to the probability density function as (Liu et al., 2018):

$$f(u) = \frac{m}{u_0} \left(\frac{u}{u_0} \right)^{m-1} e^{-\left(\frac{u}{u_0} \right)^m} \quad (12)$$

where u is the relevant mechanical parameters (e.g. elastic modulus or strength), u_0 is the mean values of the rock parameters,

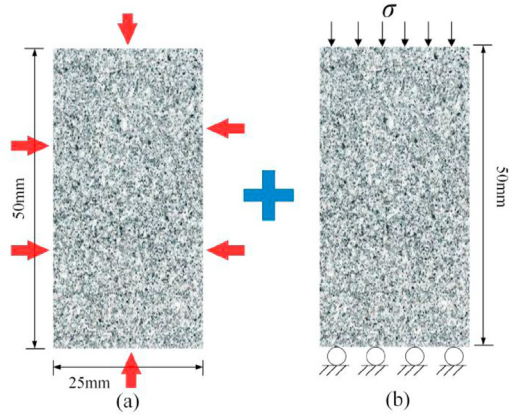


Fig. 15. Numerical modeling geometry used for full sequence of thermomechanical-damage modeling (TM(D)): (a) Thermal treatment, and (b) Uniaxial compression to failure.

and m is the shape parameter of the Weibull distribution function. Different m values correspond to different probability density distribution functions, and the data are gradually concentrated with the increase in m . The more concentrated the rock mechanical parameters are, the more homogeneous the rock properties are.

The data related to numerical simulation can be obtained through experiments, as shown in Table 2.

Because it is difficult for the numerical model to simulate the crack or pore compression closure stage of the rock, the deformation modulus $E_{50} = 15.4$ MPa is used as the initial parameter instead of the elastic modulus. The mean values of the parameters at the assignment of the Weibull distribution were obtained by calculation and substituted into the uniaxial compression model, and the initial elastic modulus distribution of the model corresponding to different values of m is shown in Fig. 16a. The stress-strain curves corresponding to different values of m are simulated and compared with the experimental results, as shown in Fig. 16b. It can be seen that the stress-strain curve in the experiment is similar to the curve simulated using the homogeneity index $m = 10$. Therefore, it is considered that the homogeneity index m of granite at room temperature is 10.

4.3. Double damage TM(D) model

4.3.1. Heat transfer and damage patterns during heating

The first step in this numerical model is to determine the elastic modulus and peak strength of the granite through the Weibull distribution function, and this method is used to represent the inhomogeneity of granite. The heat transfer distribution (left side) and damage distribution cloud (right side) of the rock from the beginning of heating to the beginning of cooling at different temperatures are shown in Fig. 17. In the damage cloud diagram, tensile damage is negative and shear damage is positive. From the figure, it can be concluded that the whole heating and holding process at 200 °C and 400 °C caused little thermal damage to the granite. When the temperature reaches 600 °C, there will be obvious thermal damage, and the damage effect becomes pronounced as the temperature rises.

Table 2

Initial parameters used in the numerical simulation.

Temperature (°C)	Density (g/cm ³)	Uniaxial compressive strength (MPa)	Deformation modulus (GPa)	Porosity (%)	Poisson's ratio	Thermal conductivity (W/(m K))
25	2.576	116.4	15.1	0.5	0.384	2.98

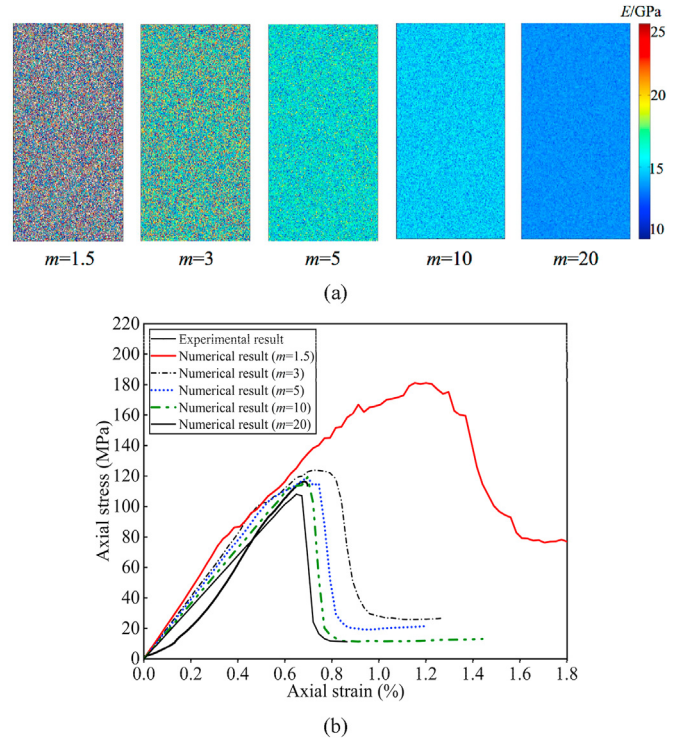


Fig. 16. Simulation of homogeneous samples: (a) Distribution of elastic modulus for different initial values of m , and (b) Stress-strain curves simulated for different values of m .

4.3.2. Damage and rupture under uniaxial loading

Fig. 18a shows the elastic modulus distribution of granite treated by high temperature. The elastic modulus remains almost constant in the temperature interval from 25 °C to 400 °C, and there is a significant decrease in elastic modulus when the temperature reaches 600 °C, which is very close to the experimental results. By the simulation of uniaxial compression, the elastic modulus distributions of heat-treated granite at the final rupture state are presented in Fig. 18b. It is obvious that with the increase in temperature, the axial deformation of granite gradually increases. Over 600 °C, the large deformation zone of rock mostly concentrates in the upper and lower ends of the rock due to the decline in the elastic modulus.

Fig. 19 presents the simulated uniaxial compressive stress-strain curves of granite under different temperatures. The peak stress and strain are summarized in Fig. 20. The peak stresses from simulation and experiment exhibit the similar trend of increasing first and then decreasing. When the temperature is below 400 °C, the results of numerical simulation are highly close to that of experiment. It should be noted that, when the temperature exceeds 400 °C, due to the possible oxidation reaction inside the rock and the phase transformation of the minerals, damage of the physical granite is much larger than that in the simulation. These cause the larger simulated results compared with that of experiment, specifically in peak axial strain.

The elastic modulus E and the deformation modulus E_{50} are measured according to the stress-strain curves from rock

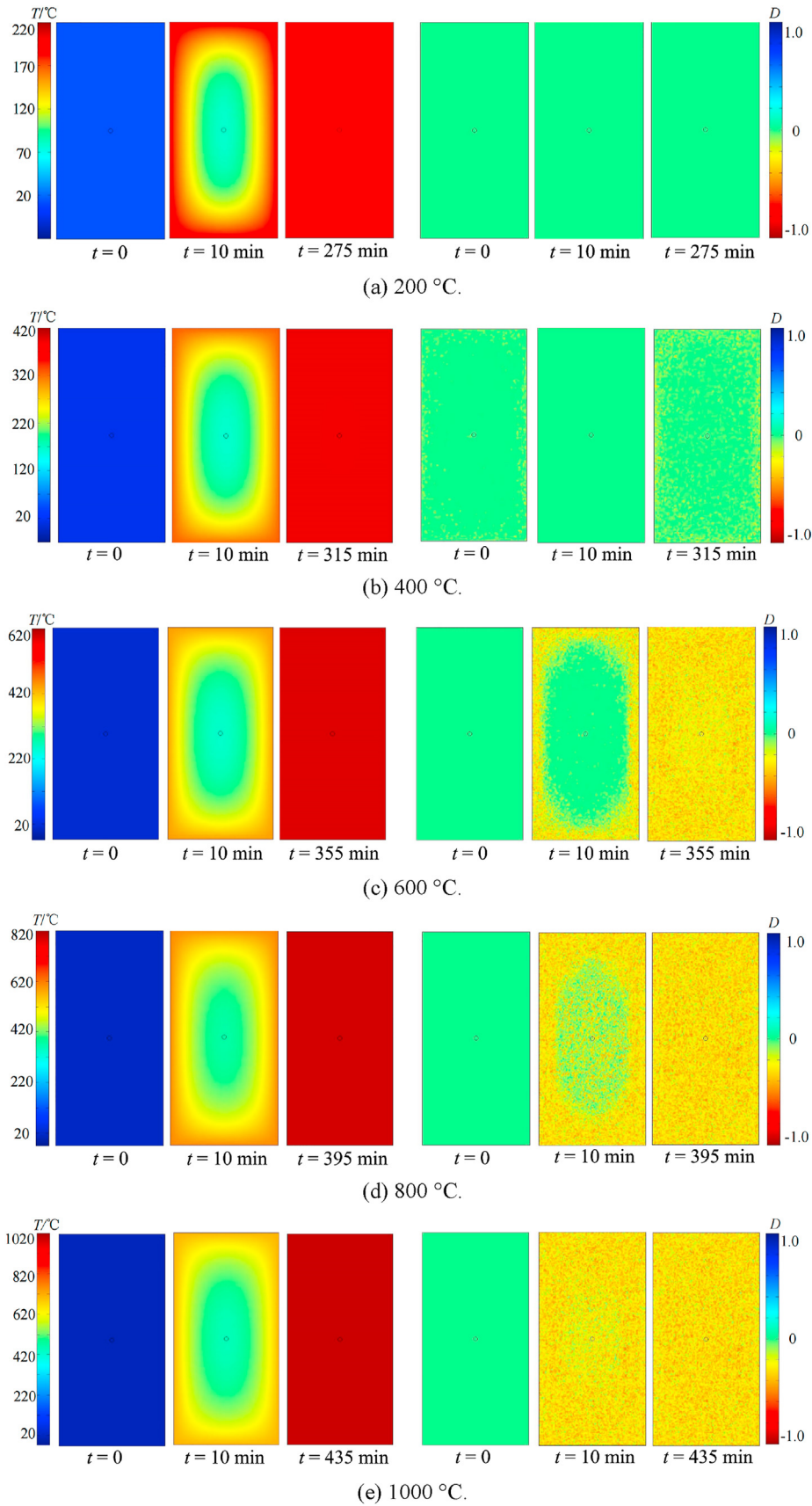


Fig. 17. Color maps of heat transfer (temperature) and damage during unstressed heating.

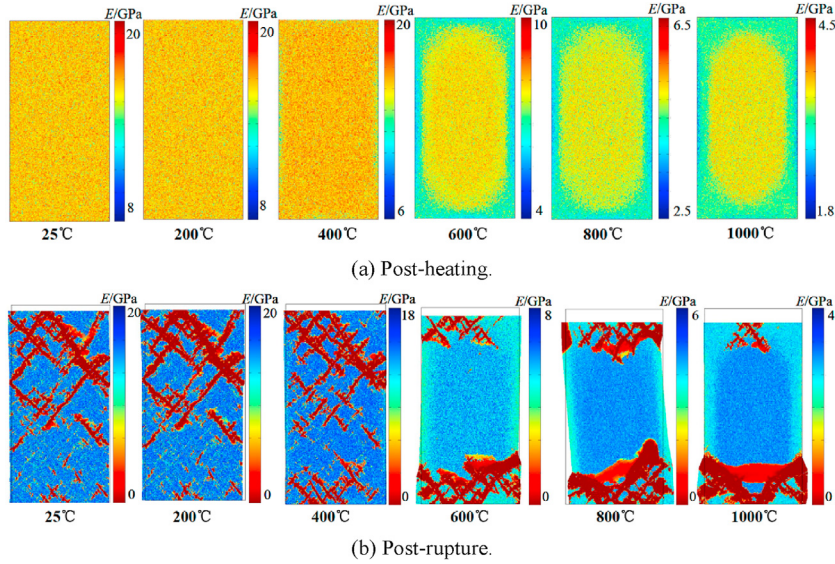


Fig. 18. Color maps of elastic modulus distribution after (a) first heating and (b) mechanical loading.

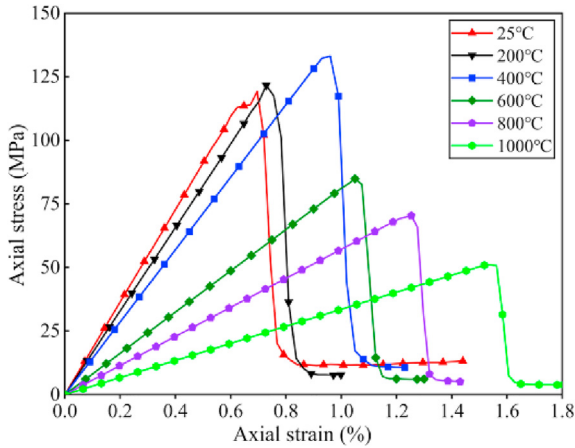


Fig. 19. Simulated uniaxial stress-strain curves for different pre-treatment temperatures.

mechanics experiments conducted after heat treatment. The elastic modulus E' at different temperatures is obtained from the numerical simulation of thermomechanical coupling based on the experimental results. Comparisons between the elastic modulus E ,

deformation modulus E_{50} , and numerical elastic modulus E' are shown in Table 3. E , E_{50} , and E' all decrease with increasing temperature, and there is a consistent trend where $E > E' > E_{50}$.

4.4. Inversion for homogeneity index m

Once the simulation for heat-treated rock is completed, the elastic modulus distribution of heat-treated granite at different temperatures can be obtained. By data integration, the probability density distribution of elastic modulus of granite at different temperatures is obtained inversely, as can be seen at Fig. 21a. Overall, the density distribution function of the elastic modulus of granite tends to gradually flatten to the left with the temperature, which

Table 3 Variations of moduli E , E' and E_{50} for different pre-treatment temperatures.

Temperature (°C)	E (GPa)	E_{50} (GPa)	E' (GPa)
25	21.76	15.13	18.19
200	20.5	12.43	16.43
400	19.6	10.64	14.25
600	13	4.43	8.11
800	9.5	2.77	5.71
1000	2.3	0.84	3.35

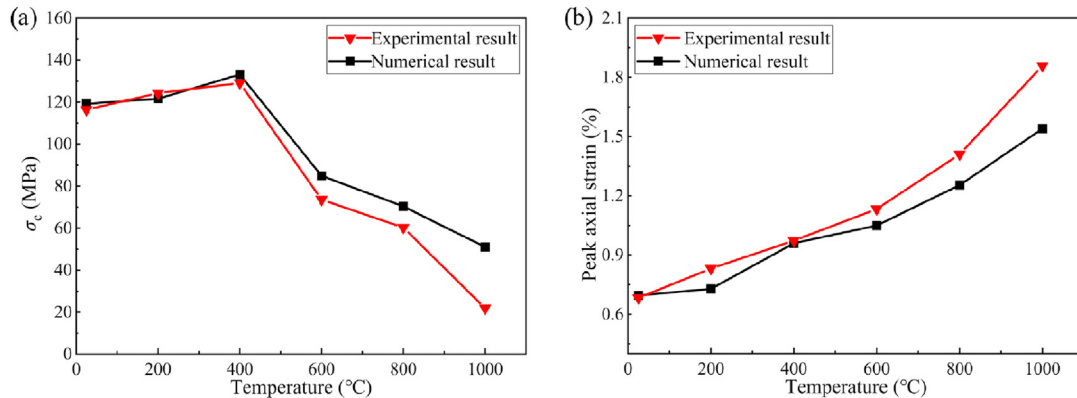


Fig. 20. Comparison of peak stress and peak strain by both experiment and simulation: (a) Peak stress, and (b) Peak axial strain.

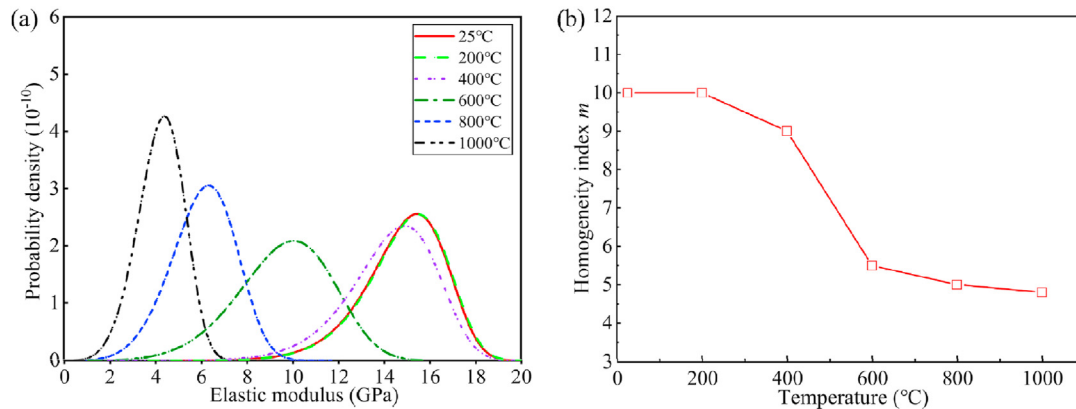


Fig. 21. Inversion results at different temperatures: (a) Probability density distribution for elastic modulus, and (b) Homogeneity index m .

indicates that the elastic modulus is decreasing with elevated temperature.

The probability density curves corresponding to different values of homogeneity index m can be plotted through the Weibull distribution. Comparing the different curves with the numerical result can determine the homogeneity index that is closest to the numerical result curve, which is the homogeneity index m after heating at specific temperature. From Fig. 21b, it can be seen that the homogeneity index m gradually decreases with increasing temperature from 10 at the room temperature to 4.57 at 1000 °C, with the largest decrease between 400 °C and 600 °C. Due to the elastic modulus damage caused by heating, the higher the temperature the more inhomogeneous the rock behaves.

5. Conclusions

The mechanical and thermodynamic characteristics of granite subjected to various high temperatures are investigated through experiments, such as XRD, NMR, SEM, uniaxial and triaxial compression tests, as well as multi-physical simulations. The evolution of mechanical parameters under different temperatures and confining pressures is studied in detail. Changes in micro-components and structure of rock across different temperatures are examined. Based on non-homogeneous damage mechanics, a dual-damage coupled TM(D) model is employed to analyze the evolution of thermal damage and mechanical degradation in granite. The conclusions are drawn as follows:

- (1) For the studied granite, 400 °C marks the threshold temperature at which changes in mass, volume, density, and porosity occur. The thermal conductivity and thermal diffusivity of granite correlate well with the rate of change in longitudinal wave velocity and the porosity. The sensitivity of the physical parameters to temperature, ranked in descending order, is as follows: longitudinal wave velocity > thermal conductivity > thermal diffusivity > volume > density > mass.
- (2) The significant increase in thermal damage after reaching 400 °C can be attributed to the decomposition of albite under high-temperature conditions. The crucial factor that contributes to the brittle-ductile transformation of granite within the temperature range of 600–800 °C is the conversion of potassium feldspar into plagioclase induced by elevated temperatures. SEM results indicate a significant increase in the number of cracks and pores when the temperature exceeds 800 °C, attributable to the thermal degradation of the crystal structure integrity of calcium feldspar.

- (3) The porosity of granite increases with rising temperature, with a significant growth rate observed beyond 400 °C. Micropores and mesopores initially decrease and then increase as the temperature rises, while macropores consistently expand. This behavior is attributed to the gradual evolution of micropores at higher temperatures.
- (4) Under uniaxial compression, the peak stress, damage stress, elastic modulus, and deformation modulus of granite indicate that 400 °C serves as the threshold temperature for granite damage. Furthermore, the ratio of damage stress to peak stress, along with the change of ductility coefficient, reveal that temperature range for the brittle-ductile transition of studied granite is approximately 600–800 °C.
- (5) The multi-physical simulation using the TM(D) coupled model aligns well with experimental results. At room temperature, the homogeneity index (m) of granite is approximately 10. However, at 600 °C, thermal damage intensifies rapidly, significantly altering the rupture morphology. In terms of elastic modulus damage, the homogeneity index (m) of granite decreases with increasing temperature, indicating that the granite's non-homogeneity increases with temperature. This demonstrates that higher temperatures lead to more inhomogeneous rock behavior.

CRedit authorship contribution statement

Liyuan Liu: Writing – original draft, Software, Project administration, Funding acquisition, Formal analysis, Conceptualization. **Shengwen Luo:** Visualization, Methodology, Investigation, Data curation. **Derek Elsworth:** Writing – review & editing, Supervision. **Kai Liu:** Writing – review & editing, Investigation. **Yifan Luo:** Software, Methodology, Investigation. **Hongguang Ji:** Supervision. **Tao Wang:** Supervision, Funding acquisition, Conceptualization.

Declaration of competing interest

The authors declare that they have no known competing financial interests or personal relationships that could have appeared to influence the work reported in this paper.

Acknowledgment

This work was funded by the Beijing Natural Science Foundation (Grant No. JQ21028), the National Natural Science Foundation of China (Grant Nos. 52311530070 and 52004015). Their support is gratefully acknowledged.

References

- Abddaim, E., Sakami, S., El Hassnaoui, A., Boukhattem, L., 2024. Impact of temperature on chemical, thermo-physical, and mechanical properties of four rock materials for sensible thermal energy storage. *J. Energy Storage* 89, 15.
- Alanazi, A., Yekeen, N., Ali, M., Abu-Mahfouz, I.S., Keshavarz, A., Iglauer, S., Hoteit, H., 2023. Influence of organics and gas mixing on hydrogen/brine and methane/brine wettability using Jordanian oil shale rocks: implications for hydrogen geological storage. *J. Energy Storage* 62, 20.
- Chen, S.W., Wang, G.B., Zuo, S.Y., Yang, C.H., 2021. Experimental investigation on microstructure and permeability of thermally treated Beishan granite. *J. Test. Eval.* 49 (2), 881–895.
- Ersoy, H., Atalar, C., Sünnetci, M.O., Kolayli, H., Karahan, M., Ersoy, A.F., 2021a. Assessment of damage on geo-mechanical and micro-structural properties of weak calcareous rocks exposed to fires using thermal treatment coefficient. *Eng. Geol.* 284, 13.
- Ersoy, H., Karahan, M., Kolayli, H., Sünnetci, M.O., 2021b. Influence of mineralogical and micro-structural changes on the physical and strength properties of post-thermal-treatment clayey rocks. *Rock Mech. Rock Eng.* 54 (2), 679–694.
- Ersoy, H., Kolayli, H., Karahan, M., Karahan, H.H., Sünnetci, M.O., 2019. Effect of thermal damage on mineralogical and strength properties of basic volcanic rocks exposed to high temperatures. *Bull. Eng. Geol. Environ.* 78 (3), 1515–1525.
- Gautam, P.K., Dwivedi, R., Kumar, A., Kumar, A., Verma, A.K., Singh, K.H., Singh, T.N., 2021. Damage characteristics of jalore granitic rocks after thermal cycling effect for nuclear waste repository. *Rock Mech. Rock Eng.* 54 (1), 235–254.
- Gautam, P.K., Verma, A.K., Jha, M.K., Sharma, P., Singh, T.N., 2018. Effect of high temperature on physical and mechanical properties of Jalore granite. *J. Appl. Geophys.* 159, 460–474.
- Hart, K.A., Rimoli, J.J., 2023. A computational model for the thermal spallation of crystalline rocks. *J. Appl. Geophys.* 56 (11), 8235–8254.
- He, M., Yu, L.Y., Liu, R.C., Jiang, Y.J., Li, Z.C., Wang, X.L., 2022. Experimental investigation on mechanical behaviors of granites after high-temperature exposure. *J. Cent. South Univ.* 29 (4), 1332–1344.
- Igusheva, L.A., Petrov, Y.V., 2024. Effect of thermal treatment on the granite dynamic fracture toughness and its structural-temporal characteristics. *Mech. Solid.* 59 (1), 379–386.
- Jin, Y.Z., He, C., Yao, C., Sun, Z.J., Wang, J.L., Zhang, X.B., Yang, J.H., Jiang, Q.H., Zhou, C.B., 2024. Experimental and numerical simulation study on the evolution of mechanical properties of granite after thermal treatment. *Comput. Geotech.* 172, 18.
- Kahraman, E., 2022. Investigation of the effects of two different cooling treatments on the physico-mechanical and microstructural properties of granite after high temperatures. *Geomech. Geophys. Geo-Energy Geo-Resour.* 8 (5), 20.
- Kumari, W.G.P., Beaumont, D.M., Ranjith, P.G., Perera, M.S.A., Isaka, B.L.A., Khandelwal, M., 2019. An experimental study on tensile characteristics of granite rocks exposed to different high-temperature treatments. *Geomech. Geophys. Geo-Energy Geo-Resour.* 5 (1), 47–64.
- Kumari, W.G.P., Ranjith, P.G., 2022. Experimental and numerical investigation of the flow behaviour of fractured granite under extreme temperature and pressure conditions. *Sustainability* 14 (14), 19.
- Lan, H.X., Martin, C.D., Andersson, J.C., 2013. Evolution of in situ rock mass damage induced by mechanical-thermal loading. *Rock Mech. Rock Eng.* 46 (1), 153–168.
- Li, C.Z., Chen, G.J., Li, C., Tian, B., Sun, R., Su, L., Lu, Y.X., Wang, L.J., 2021. Experimental study on water-rock reactions with CO₂ fluid in a deep sandstone formation under high temperature and pressure. *Acta Geol. Sin.-Engl. Ed.* 95 (1), 268–279.
- Li, M.Y., Wu, Z.J., Weng, L., Liu, Q.S., Chu, Z.F., 2022. Quantitative relationships between the mineral composition and macro mechanical behaviors of granite under different temperatures: insights from mesostructure-based DEM investigations. *Comput. Geotech.* 148, 20.
- Li, X.W., Lin, J., Shao, W.H., Ge, D.L., Wu, Y., 2024. Study on the evolution law of physical mechanics and abrasion characteristics of granite under high temperature-water cooling treatment. *Case Stud. Therm. Eng.* 58, 12.
- Li, M.Y., Zhang, F.S., 2024. Modeling the fracturing behavior transition in fractured granite under thermo-hydro-mechanical (THM) condition. *GeoShanghai Int. Conf.* 1331 (2).
- Liu, L.Y., Ji, H.G., Elsworth, D., Zhi, S., Lv, X.F., Wang, T., 2020. Dual-damage constitutive model to define thermal damage in rock. *Int. J. Rock Mech. Min. Sci.* 126, 12.
- Liu, L.Y., Ji, H.G., Lu, X.F., Wang, T., Zhi, S., Pei, F., Quan, D.L., 2021. Mitigation of greenhouse gases released from mining activities: a review. *Int. J. Miner. Metall. Mater.* 28 (4), 513–521.
- Liu, L.Y., Jin, J., Liu, J.D., Cheng, W., Zhao, M.H., Luo, S.W., Luo, Y.F., Wang, T., 2025. Mechanical properties of sandstone under in-situ high-temperature and confinement conditions. *Int. J. Miner. Metall. Mater.* 32 (4), 778–787.
- Liu, L.Y., Li, L.C., Elsworth, D., Zhi, S., Yu, Y.J., 2018. The impact of oriented perforations on fracture propagation and complexity in hydraulic fracturing. *Processes* 6 (11), 19.
- Liu, Z.X., Wu, Y., Li, X.Z., Huang, Z., Lin, J., Pan, X.H., 2022. Effects of thermal treatment on the macroscopic physical properties and microstructure of Beishan fine-grained granite. *Bull. Eng. Geol. Environ.* 81 (5), 18.
- Meng, T., Meng, X.X., Donghua, Z.H., Hu, Y.Q., 2018. Using micro-computed tomography and scanning electron microscopy to assess the morphological evolution and fractal dimension of a salt-gypsum rock subjected to a coupled thermal-hydrological-chemical environment. *Mar. Petrol. Geol.* 98, 316–334.
- Nie, W., Wang, J.L., Feng, C., Zhang, Y.M., 2023. Continuous-discontinuous element method for three-dimensional thermal cracking of rocks. *J. Rock Mech. Geotech. Eng.* 15 (11), 2917–2929.
- Pathiranagei, S.V., Gratchev, I., 2021. Engineering properties of sandstone heated to a range of high temperatures. *Bull. Eng. Geol. Environ.* 80 (3), 2415–2432.
- Peng, L., Li, X.L., Peng, X., Gan, Y.C., Wang, J.G., 2024. Analysis of physical and mechanical behaviors and microscopic mineral characteristics of thermally damaged granite. *Sci. Rep.* 14 (1), 21.
- Saksala, T., 2021. Numerical modeling of thermo-mechanical failure processes in granitic rock with polygonal finite elements. *Int. J. Numer. Anal. Methods Geomech.* 45 (13), 1900–1919.
- Sun, W., Wu, S.C., Xu, X.L., 2021. Mechanical behaviour of Lac du Bonnet granite after high-temperature treatment using bonded-particle model and moment tensor. *Comput. Geotech.* 135, 22.
- Wang, T., Ye, W.W., Liu, L.Y., Liu, K., Jiang, N.S., Feng, X.H., 2024. Disturbance failure mechanism of highly stressed rock in deep excavation: current status and prospects. *Int. J. Miner. Metall. Mater.* 31 (4), 611–627.
- Wu, Y., Hu, L.H., Yu, J., Li, X.Z., Yang, L.N., Xue, S., Zhang, K., 2023. The sensitivity of physical properties and pore structures of Beishan granite to large variation of temperature in nuclear waste storage sites. *Environ. Sci. Pollut. Res.* 30 (30), 75195–75212.
- Xi, Y., Wang, H.Y., Zha, C.Q., Li, J., Guo, B.Y., 2022. Experimental study of the influence of temperature and cooling method on dynamic mechanical properties and damage of granite. *Energy Sci. Eng.* 10 (10), 3779–3797.
- Xie, H.P., Gao, M.Z., Fu, C.H., Lu, Y.Q., Yang, M.Q., Hu, J.J., Yang, B.G., 2021. Mechanical behavior of brittle-ductile transition in rocks at different depths. *J. China Coal Soc.* 46 (3), 701–715.
- Yang, J., Fu, L.Y., Zhang, W.Q., Wang, Z.W., 2019. Mechanical property and thermal damage factor of limestone at high temperature. *Int. J. Rock Mech. Min. Sci.* 117, 11–19.
- Zhang, J.Y., Shen, Y.J., Yang, G.S., Zhang, H., Wang, Y.Z., Hou, X., Sun, Q., Li, G.Y., 2021. Inconsistency of changes in uniaxial compressive strength and P-wave velocity of sandstone after temperature treatments. *J. Rock Mech. Geotech. Eng.* 13 (1), 143–153.
- Zhu, W.C., Tang, C.A., 2004. Micromechanical model for simulating the fracture process of rock. *Rock Mech. Rock Eng.* 37 (1), 25–56.



Liyuan Liu serves as an Associate Professor at the University of Science and Technology Beijing. He earned his PhD in Mining Engineering from Northeastern University of China in 2018, under the mentorship of Prof. Wancheng Zhu and Prof. Derek Elsworth. His research delves into the Rock Damage Mechanism under Multi-Physical Field Coupling, with expertise spanning computational mechanics, geomechanics, and geophysics. A significant focus of his work is on induced seismicity and its effects on the mechanical and transport properties of fractured rocks — research with vital applications in mining engineering, geothermal energy, and the deep geological storage of radioactive waste and CO₂. Acknowledged for his contributions, he has been awarded distinctions such as the China Postdoctoral Innovative Talent Support Program and the Beijing Young Talent Support Initiative.